Chinese Journal of Physics 91 (2024) 867–882

Contents lists available at ScienceDirect

Chinese Journal of Physics

journal homepage: www.sciencedirect.com/journal/chinese-journal-of-physics

Transition to chaotic flow, bifurcation, and entropy generation analysis inside a stratified trapezoidal enclosure for varying aspect ratio

Md. Mahafujur Rahaman [a,b], Sidhartha Bhowmick [a], Goutam Saha [c,d], Feng Xu [e], Suvash C. Saha [d,*]

[a] Department of Mathematics, Jagannath University, Dhaka 1100, Bangladesh
[b] Department of Computer Science and Engineering, Z. H. Sikder University of Science and Technology, Shariatpur 8024, Bangladesh
[c] Department of Mathematics, University of Dhaka, Dhaka 1000, Bangladesh
[d] School of Mechanical and Mechatronic Engineering, University of Technology Sydney, Ultimo, North South Wales, 2007, Australia
[e] School of Civil Engineering, Beijing Jiaotong University, Beijing, 100044, China

ARTICLE INFO

Keywords:
Aspect ratio
Natural convection
Entropy generation
Stratified fluid
Heat transfer
Bejan number

ABSTRACT

In this numerical study, we investigate the effect of aspect ratio (*AR*) on the natural convection (NC) flow and entropy generation (S_{gen}) in a stratified fluid confined inside a trapezoidal enclosure with thermally stratified side walls. The bottom of the enclosure is heated, and top of the enclosure is cooled. We use the Finite Volume Method (FVM) for simulating unsteady flows. We consider a Prandtl number (Pr = 0.71 for air) and explore *AR* of 0.2, 0.5, and 1.0, covering a wide range of Grashof numbers (Gr) from 10 to 10^8. The outcomes are presented for Grashof numbers and the effect of the *AR* on fluid flow, rates of heat transfer (HT), and S_{gen} inside the enclosure. Critical Grashof numbers are identified, marking the shift in flow behavior from being influenced by baroclinic to Rayleigh–Bénard instability, and from a steady to an unsteady state for various *AR*. In the context of this transition to chaotic flow, several supercritical bifurcations are observed, including a Pitchfork bifurcation from symmetric to asymmetric states and a Hopf bifurcation from a steady state to an unsteady state. Additionally, we analyze the discrepancies in average entropy generation (S_{avg}) and average Bejan number (Be_{avg}) across the entire enclosure, considering various *AR* and Gr values. It is observed that for enclosures with Gr $\geq 10^5$, S_{avg} increases as *AR* decreases, indicating an enhancement in HT rate with decreasing *AR*. Furthermore, a quantitative relationship between S_{avg}, HT, *AR*, and Gr is presented. The study concludes that, as *AR* increases, the ecological coefficient of performance (*ECOP*) decreases, signifying a reduction in thermodynamics efficiency.

1. Introduction

Natural convection (NC) is a ubiquitous phenomenon in our environment, and most free convection flows, especially those observed in engineering applications, exhibit unsteadiness. Over the past few decades, there has been a growing interest in unsteady NC for two main reasons: firstly, the necessity to achieve a deeper understanding of unsteady NC from a phenomenological perspective,

* Corresponding author.
E-mail address: Suvash.Saha@uts.edu.au (S.C. Saha).

https://doi.org/10.1016/j.cjph.2024.08.034
Received 25 May 2024; Received in revised form 21 August 2024; Accepted 25 August 2024
Available online 26 August 2024

Nomenclature

AR	aspect ratio
L, H	half-length and height of the cavity (m)
g	gravitational force (m/s^2)
t	time (s)
Cp	specific heat (J/kgK)
P	pressure (N/m^2)
p	dimensionless pressure
T	temperature (K)
T_∞	environmental temperature (K)
T_h	temperature of the bottom surface (K)
T_c	temperature of the top surface (K)
T_i	temperature of the inclined surface (K)
ΔT	temperature difference, $(T_h - T_c)$
Gr	Grashof number, $g\beta(T_h\text{-}T_c)H^3/\nu^2$
Pr	Prandtl number
S_{gen}	entropy generation
Nu	Nusselt number
S_f	entropy generation due to fluid friction
S_t	local entropy generation
Nu_{avg}	average Nusselt number
S_{avg}	average entropy generation
Be	Bejan number
Be_l	local Bejan number
Be_{avg}	average Bejan number
X, Y	coordinates
x, y	dimensionless coordinates
U, V	velocity components (m/s)
u, v	dimensionless velocity components
k	thermal conductivity (W/mK)

Greek symbols

θ	dimensionless temperature
ν	kinematic viscosity (m^2/s)
ρ	density (kg/m^3)
S_θ	entropy generation due to heat transfer
κ	thermal diffusivity (m^2/s)
φ	irreversibility distribution ratio
τ	dimensionless time
$\Delta\tau$	dimensionless time step
θ_c	dimensionless temperature of the top surface
θ_h	dimensionless temperature of the bottom surface
θ_i	dimensionless temperature of the inclined surface

and secondly, the pressing need for accurate numerical models to predict the corresponding flow configurations and associated heat transfer (HT) in industrial operations. In natural systems, such as the atmosphere, the ocean, and various technical contexts, HT mechanisms through NC in stratified media are common. Despite its significant impact on heat dissipation processes, only a limited number of studies addressing this phenomenon can be found in the literature. One such study investigated NC occurring around an isothermal plate submerged in a stably stratified fluid across a wide range of thermal stratification levels [1]. This research utilized boundary layer (BL) approximations and solved two-dimensional partial differential equations using the finite-difference method. However, it was found that these BL analyses were inaccurate for NC flows in stratified fluids, especially at high stratification levels characterized by steep temperature increases with respect to height. To achieve accurate solutions and gain a comprehensive understanding of the physical mechanisms involved, another study examined free convection HT within a low porosity medium saturated with a stably stratified fluid, where Darcy flow dominates [2]. Further investigations by different researchers explored the impact of stratification on convection in various geometries, including vertical circular cones, isothermal semi-infinite plates, and single infinite vertical plates [3–6]. These studies included analytical solutions for Prandtl numbers (Pr) of unity, impulsive temperature changes, and variations in heat flux.

In industrial settings, NC flows are typically unsteady, prompting extensive research on the transition of NC flows in cavities

subjected to sudden heating and cooling. Patterson and Imberger [7] were among the first to discuss the features of unsteady NC flows in enclosures, emphasizing vertical boundary layer flow, horizontal intrusion flow, and core flow. Subsequently, various researchers [8–11] have conducted comprehensive investigations on regular enclosures using numerical models, providing fundamental comprehension of mixed convection, transient NC flows and HT characteristics. Traditionally, it is assumed that the flow within enclosures is symmetric along the centerline. However, the observation of a pitchfork bifurcation under nighttime cooling conditions led to the discovery of asymmetric flow patterns in isosceles triangular enclosures by several researchers [12–14]. These findings challenged the previously held belief of symmetry in flow patterns and prompted further research. Researchers investigated the impact of *ARs* and Rayleigh numbers (Ra) on NC in various cavity shapes, including triangular and isosceles triangular configurations [15–17]. These studies offered valuable insights into the influence of geometry on fluid flow and HT. Similarly, the behavior of NC flow in different enclosure shapes under varying conditions, such as heat flux variation and diurnal temperature fluctuations also been investigated [18–21].

In many engineering applications, variations in enclosure geometry, such as Z-shaped enclosure [22], zigzag configurations [23], arc shape [24], and enclosure containing fixed and moving rigid bodies [25], introduce significant complexity to the analysis. Among these, the investigation of NC within trapezoidal enclosures presenting the greatest challenge due to their inclined walls. Iyican et al. [26,27] were among the first to explore NC in trapezoids, observing changing flow patterns from conduction to single-celled to multicellular as Ra increased. Natarajan et al. [28,29], on the other hand, conducted a computational simulation of NC in an enclosure with linearly heated side surfaces and a base surface with varying temperature conditions. Their study provided valuable insights into the impact of geometry and boundary conditions. Lasfer et al. [30] conducted laminar NC inside a trapezoidal enclosure with heated side surfaces positioned at various inclinations. They observed that HT is influenced by the flow pattern, *AR*, angle of inclination, and Ra values. Other studies have investigated NC flow in trapezoidal enclosures under various conditions, shedding light on the influence of geometry, heating, and cooling on heat transfer [31–33]. Gowda et al. [34] studied NC within a trapezoidal enclosure, where the bottom surface was partially heated, the top surface remained adiabatic, and the inclined surface was kept at a constant cool temperature. This investigation enabled them to gain insights into how the length of heating along the active bottom wall affected convection. Recently, Rahaman et al. [35–37] explored transient NC flows inside a trapezoidal enclosure initially filled with stratified and non-stratified air, with adiabatic side walls. Subsequently, Rahaman et al. [38] investigated further to understand transient NC flow in the same geometry, with thermally stratified air and stratified inclined walls.

The study of NC not only provides insight into HT mechanisms influenced by fluid properties, *ARs*, and boundary conditions, but also extends to the investigation of entropy generation (S_{gen}) within the system. Entropy generation is directly related to the loss of available energy and the increase in energy wastage. Bejan [39,40] introduced the concept of minimizing S_{gen}, guided by the second law of thermodynamics. Numerous studies have presented S_{gen} resulting from HT and fluid friction (FF) irreversibilities in various enclosures during natural convection [41–45].

The analysis of the literature reveals that the effect of *ARs* on S_{gen} and NC inside a trapezoidal enclosure, primarily filled with stratified air and containing a heated bottom wall, a cooled top wall, and inclined stratified walls, has not been thoroughly explored in unsteady cases before. To address this gap, a unique initiative has been undertaken in the current study to examine how *ARs* affect fluid flow, HT, and S_{gen} due to HT and FF during NC inside a trapezoidal enclosure. Within this study, two-dimensional numerical simulations are conducted for Gr ranging from 10 to 10^8, Pr of 0.71, and *ARs* of 0.2, 0.5, and 1.0. The current configuration and boundary conditions of the proposed problem fits in the valley, especially geophysical environments where the cavity geometry varies or contains additional inclining walls. The prime objective of this research is to make a comprehensive analysis of the effect of *AR* on NC and S_{gen}. Also, this research aims to identify critical Gr for all *ARs* that signifies the transition involving pitchfork bifurcation, Hopf bifurcation, and another bifurcation from periodic to chaotic states. Furthermore, the influence of Gr and *AR* on S_{gen} is emphasized, underscoring its significance in optimizing thermodynamic efficiency in NC and HT processes within these systems.

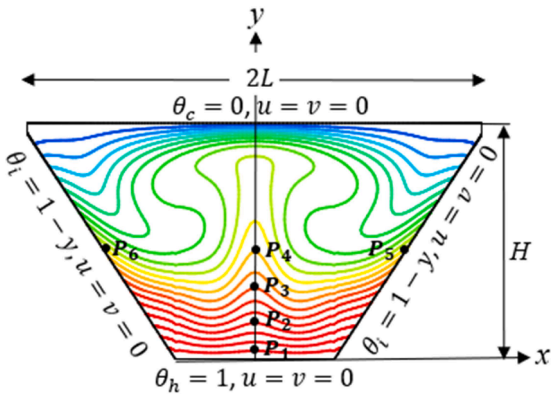

Fig. 1. Physical domain and normalized boundary conditions with results monitoring points P_1 (0, 0.13), P_2 (0, 0.27), P_3 (0, 0.40), P_4 (0, 0.53), P_5 (0.67, 0.53), and P_6 (-0.67, 0.53) are used in the derived figures.

2. Physical model

In the schematic representation shown in Fig. 1, the bottom surface of the enclosure maintains a constant temperature, denoted as T_h, which is higher than the temperature at the top, represented as T_c. The sloped walls exhibit thermal stratification. This study examines a trapezoidal enclosure with a height labeled as H, and the horizontal length of its top defined as $2L$. In Fig. 1, where $L = H$, i.e., the aspect ratio (AR) is $H/L = 1.0$. Three aspect ratios are considered: 0.2, 0.5, and 1.0 (where, for $AR = 0.5$, $L = 2H$, and for $AR = 0.2$, $L = 5H$). In all three ARs, the height H remains constant while the length L varies. To prevent singularity issues at the corner points of the inclined and top surfaces, small portions at the two top corners (4 % of L) were excluded. Two tips are considered adiabatic. The fluid within the enclosure, characterized by Pr equal to 0.71, is initially thermally stratified. All boundary walls are rigid and exhibit non-slip conditions. Also, properties of stratified fluid is presented in Table 1.

The development of 2D natural convection flow within the enclosure is governed by the Navier–Stokes equations under the Boussinesq approximation as well as energy [36]. In this study, pressure is assumed to be constant, and thermal radiation effects are not considered.

$$\begin{cases} \dfrac{\partial U}{\partial X}+\dfrac{\partial V}{\partial Y}=0, \\ \dfrac{\partial U}{\partial t}+U\dfrac{\partial U}{\partial X}+V\dfrac{\partial U}{\partial Y}=-\dfrac{1}{\rho}\dfrac{\partial P}{\partial X}+\nu\left(\dfrac{\partial^2 U}{\partial X^2}+\dfrac{\partial^2 U}{\partial Y^2}\right), \\ \dfrac{\partial V}{\partial t}+U\dfrac{\partial V}{\partial X}+V\dfrac{\partial V}{\partial Y}=-\dfrac{1}{\rho}\dfrac{\partial P}{\partial Y}+\nu\left(\dfrac{\partial^2 V}{\partial X^2}+\dfrac{\partial^2 V}{\partial Y^2}\right)+g\beta(T-T_\infty), \\ \dfrac{\partial T}{\partial t}+U\dfrac{\partial T}{\partial X}+V\dfrac{\partial T}{\partial Y}=\kappa\left(\dfrac{\partial^2 T}{\partial X^2}+\dfrac{\partial^2 T}{\partial Y^2}\right). \end{cases} \tag{1}$$

The dimensional boundary conditions are:

$$\begin{cases} \text{Top cold wall}: \quad T=T_c,\ U=V=0, \\ \text{Bottom heated wall}: \quad T=T_h,\ U=V=0, \\ \text{Inclined stratified walls}: \quad T=T_i,\ U=V=0. \end{cases} \tag{2}$$

The subsequent are the normalized variables:

$$x=\frac{X}{H},\ y=\frac{Y}{H},\ u=\frac{U}{U_c},v=\frac{V}{U_c},\ p=\frac{P}{\rho U_c^2},\ \theta=\frac{T-T_\infty}{T_h-T_c},\ \tau=\frac{tU_c}{H}\ . \tag{3}$$

Here, u, v, x, y, p, τ, and θ are the normalized form of U, V, X, Y, P, t and T. Also, $U_c=\sqrt{g\beta\Delta TH}$ is the convective velocity, and $\Delta T = T_h - T_c$.

The natural convective flow inside the enclosure is govern by three normalized parameters: Gr, Pr, and AR [35,36]:

$$\mathrm{Gr}=\frac{g\beta(T_h-T_c)H^3}{\nu^2},\mathrm{Pr}=\frac{\nu}{\kappa},\ AR=\frac{H}{L}\ . \tag{4}$$

The normalized form of the Eq. (1) is (for details refer to [46]):

Table 1
Properties of stratified fluid [38,48].

Property (unit)	Stratified fluid (Air)
Density, ρ (kg/m^3)	1.177
Specific heat, C_p (J/kgK)	1012
Viscosity, μ (kg/ms)	1.8093×10^{-5}
Thermal conductivity, k (W/mK)	0.0257887

$$\begin{cases} \dfrac{\partial u}{\partial x}+\dfrac{\partial v}{\partial y}=0, \\ \dfrac{\partial u}{\partial \tau}+u\dfrac{\partial u}{\partial x}+v\dfrac{\partial u}{\partial y}=-\dfrac{\partial p}{\partial x}+\dfrac{1}{\sqrt{\mathrm{Gr}}}\left(\dfrac{\partial^2 u}{\partial x^2}+\dfrac{\partial^2 u}{\partial y^2}\right), \\ \dfrac{\partial v}{\partial \tau}+u\dfrac{\partial v}{\partial x}+v\dfrac{\partial v}{\partial y}=-\dfrac{\partial p}{\partial y}+\dfrac{1}{\sqrt{\mathrm{Gr}}}\left(\dfrac{\partial^2 v}{\partial x^2}+\dfrac{\partial^2 v}{\partial y^2}\right)+\theta, \\ \dfrac{\partial \theta}{\partial \tau}+u\dfrac{\partial \theta}{\partial x}+v\dfrac{\partial \theta}{\partial y}=\dfrac{1}{\mathrm{Pr}\sqrt{\mathrm{Gr}}}\left(\dfrac{\partial^2 \theta}{\partial x^2}+\dfrac{\partial^2 \theta}{\partial y^2}\right). \end{cases} \tag{5}$$

The normalized boundary conditions are:

$$\begin{cases} \text{Top cold wall}: \quad \theta_c = u = v = 0, \\ \text{Bottom heated wall}: \quad \theta_h = 1,\ u = v = 0, \\ \text{Inclined stratified walls}: \quad \theta_i = 1 - y,\ u = v = 0. \end{cases} \tag{6}$$

The average Nusselt number (Nu_{avg}) on the bottom wall is defined as [38]:

$$\mathrm{Nu}_{avg} = \frac{1}{l}\int_0^1 \frac{\partial \theta}{\partial y}dx. \tag{7}$$

In a natural convection system, irreversibility arises from HT and FF. In accordance with the local thermodynamic equilibrium postulated by linear transport theory [40], the normalized local S_{gen} resulting from HT and FF and can be expressed explicitly as:

$$\begin{cases} S_\theta = \left(\dfrac{\partial \theta}{\partial x}\right)^2 + \left(\dfrac{\partial \theta}{\partial y}\right)^2, \\ S_f = \varphi\left[2\left\{\left(\dfrac{\partial u}{\partial x}\right)^2 + \left(\dfrac{\partial v}{\partial y}\right)^2\right\} + \left(\dfrac{\partial u}{\partial y}+\dfrac{dv}{dx}\right)^2\right]. \end{cases} \tag{8}$$

where, S_θ and S_f denote the S_t resulting from the HT and the FF, respectively and φ is referred to as the irreversibility distribution ratio and is defined as:

$$\varphi = \frac{\mu T_\infty}{k}\left(\frac{\kappa}{L\Delta T}\right)^2. \tag{9}$$

The local entropy generation within the cavity, denoted as S_t, results from the sum of entropy generation (S_{gen}) due to HT (S_θ) and S_{gen} due to FF (S_f):

$$S_t = S_\theta + S_f\ . \tag{10}$$

The local Bejan number (Be_l) is defined as follows [43]:

$$Be_l = \frac{S_\theta}{S_\theta + S_f}\ . \tag{11}$$

The average entropy generation (S_{avg}) and average Bejan number (Be_{avg}) are defined as [47]:

$$\begin{cases} S_{avg} = \dfrac{\int_0^1\int_0^1 S_t\,dx\,dy}{\int_0^1\int_0^1 dx\,dy}, \\ Be_{avg} = \dfrac{\int_0^1\int_0^1 Be_l\,dx\,dy}{\int_0^1\int_0^1 dx\,dy}\ . \end{cases} \tag{12}$$

The ecological coefficient of performance (*ECOP*) is defined as [47]:

$$ECOP = \frac{\mathrm{Nu}_{avg}}{S_{avg}}\ . \tag{13}$$

3. Numerical approach, grid test and validation

3.1. Methodology

The governing equations (5), along with their corresponding boundary conditions (Eqs. 6), are discretized using the Finite Volume

method [49–51], and the commercial software Fluent is employed to solve (Eqs. (5) and (6). To address the pressure-velocity coupling problem, the SIMPLE scheme is applied. Viscous terms are discretized utilizing a second-order central differencing technique, whereas advection terms are discretized using a third-order realistic QUICK scheme. In this study, a non-uniform rectangular grid arrangement is utilized, and under-relaxation factors are applied during the iteration of the discretized equations [14,17]. Convergence criteria for continuity, momentum, and energy equations are measured with a relative tolerance of 10^{-5}.

3.2. Grid test

The accuracy and constancy of numerical models are greatly affected by the grid size employed inside the computational domain. Grid and time step dependence tests have been carried out to assess the suitability of numerical methods for highest Gr. These tests were carried out using three distinct grid configurations and two time steps for each *AR* of 0.2, 0.5, and 1.0. The grid sizes selected for comparison were 300 × 75, 400 × 100 and 500 × 125 for *AR*= 0.2; 225 × 75, 300 × 100, and 375 × 125 for *AR*= 0.5; and 150 × 75, 200 × 100, and 250 × 125 for *AR*= 1.0. Additionally, time steps of 0.01 and 0.005 were chosen. The outcomes of the grid and time step dependency tests, displayed in Fig. 2, show the *u*-velocity at positions within the enclosure where the flow is the most unstable. As depicted in Fig. 2, the calculated *u*-velocity for the three grids and two-time steps initially deviates during the early transitional stage but nearly coincides during the fully developed stage (FDS) for each aspect ratio. Based on the results of these tests, it was concluded that any of the grid configurations used were suitably fine for accurately resolving the flow. Consequently, grid sizes of 400 × 100, 300 × 100, and 200 × 100, along with a time step of 0.01, were chosen for the numerical simulations corresponding to *ARs* of 0.2, 0.5, and 1.0, respectively.

3.3. Validation

To ensure the validity of the current model and findings, present results are compared with experimental results obtained by Iyican et al. [27] and Lei et al. [10], as well as numerical findings presented by Lasfer et al. [30]. Quantitative validation results of Nu_{avg} are presented in Table 2. The comparison is conducted using the dimensionless parameters Pr= 0.7, Gr values ranging from 1.41×10^3 to 1.41×10^7, and an inclination angle of 90°. Moreover, qualitative validation findings of isotherm profiles are depicted in Fig. 3. For the contrast, a reference temperature of T_∞= 293.5 K is considered, along with a Pr of 7.06 for water, and a Grashof number of 2.36×10^5 determined by adjusting the temperatures to T_h= 297.5 K and T_c= 289.5 K. These comparisons demonstrate remarkable concurrence.

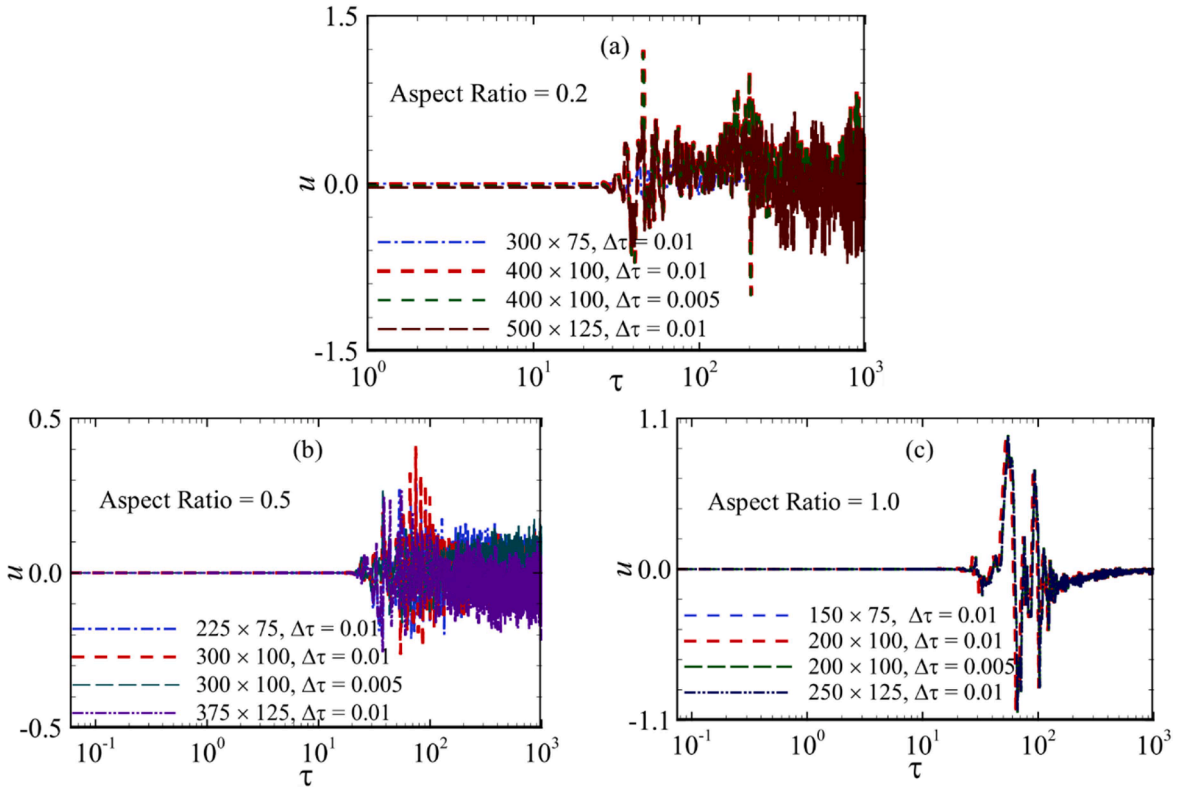

Fig. 2. Grid and time step dependent tests for *AR* of 0.2, 0.5, and 1.0 at point P_1 (0, 0.13) for Gr= $10^{8.}$

Table 2
Nu_{avg} results for different Gr.

Gr	Experimental [27]	Numerical [30]	Present study
1.41×10^3	–	1.66	1.56
1.41×10^4	2.20	2.33	2.31
1.41×10^5	5.20	6.09	5.99
1.41×10^6	12.50	13.40	13.10
1.41×10^7	29.52	–	29.21

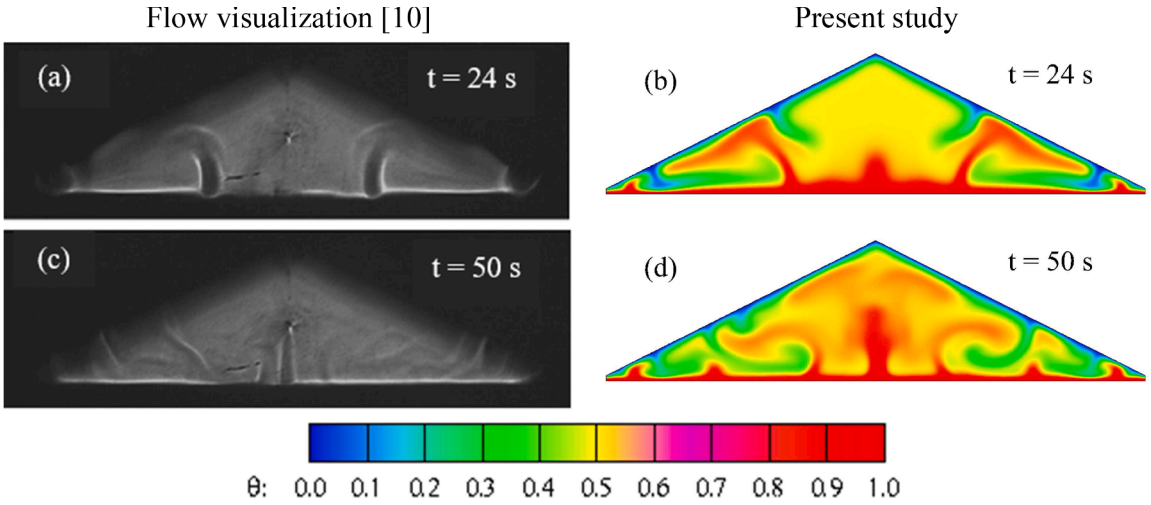

Fig. 3. Isotherm profiles at a fixed Gr (Gr= 2.36×10^5).

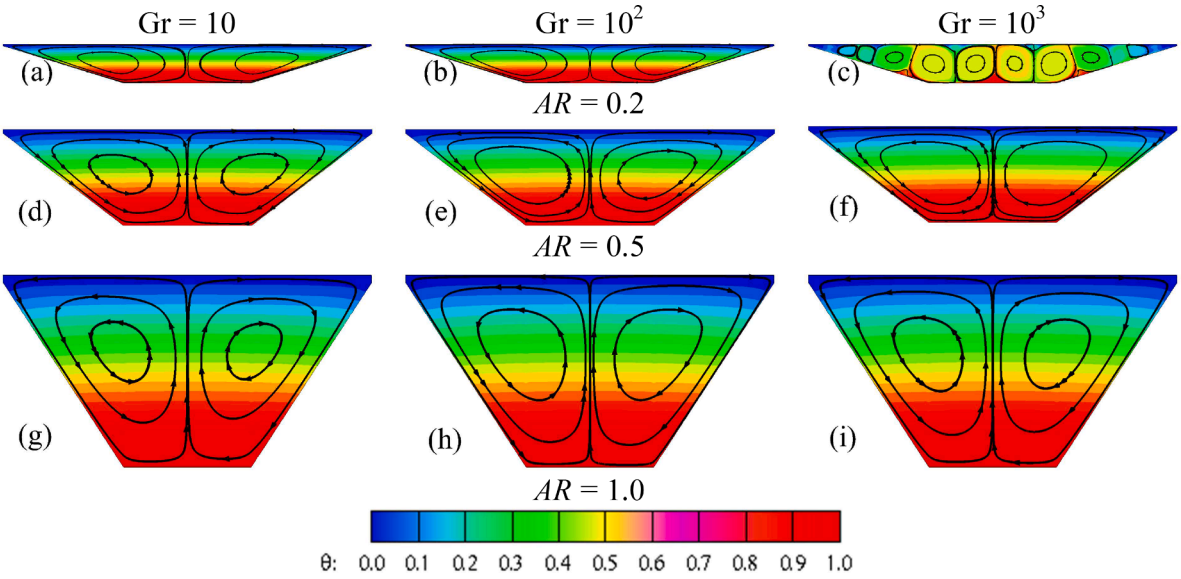

Fig. 4. Streamlines and isotherms to observe the NC flows for different aspect ratios.

4. Results and discussion

This study explores the impact of *AR* on the unsteady NC and S_{gen} within a stratified trapezoidal enclosure. Numerical simulations are conducted for three *ARs*: 0.2, 0.5, and 1.0, with Pr set to 0.71, covering a wide range of Gr from 10 to 10^8. These dominant dimensionless parameters, including *AR* and Pr, encompass various interesting transitional flow patterns. The unique aspect of this study is its identification of critical Gr that signify transitions to asymmetric, periodic, and chaotic states at different *ARs*. Additionally,

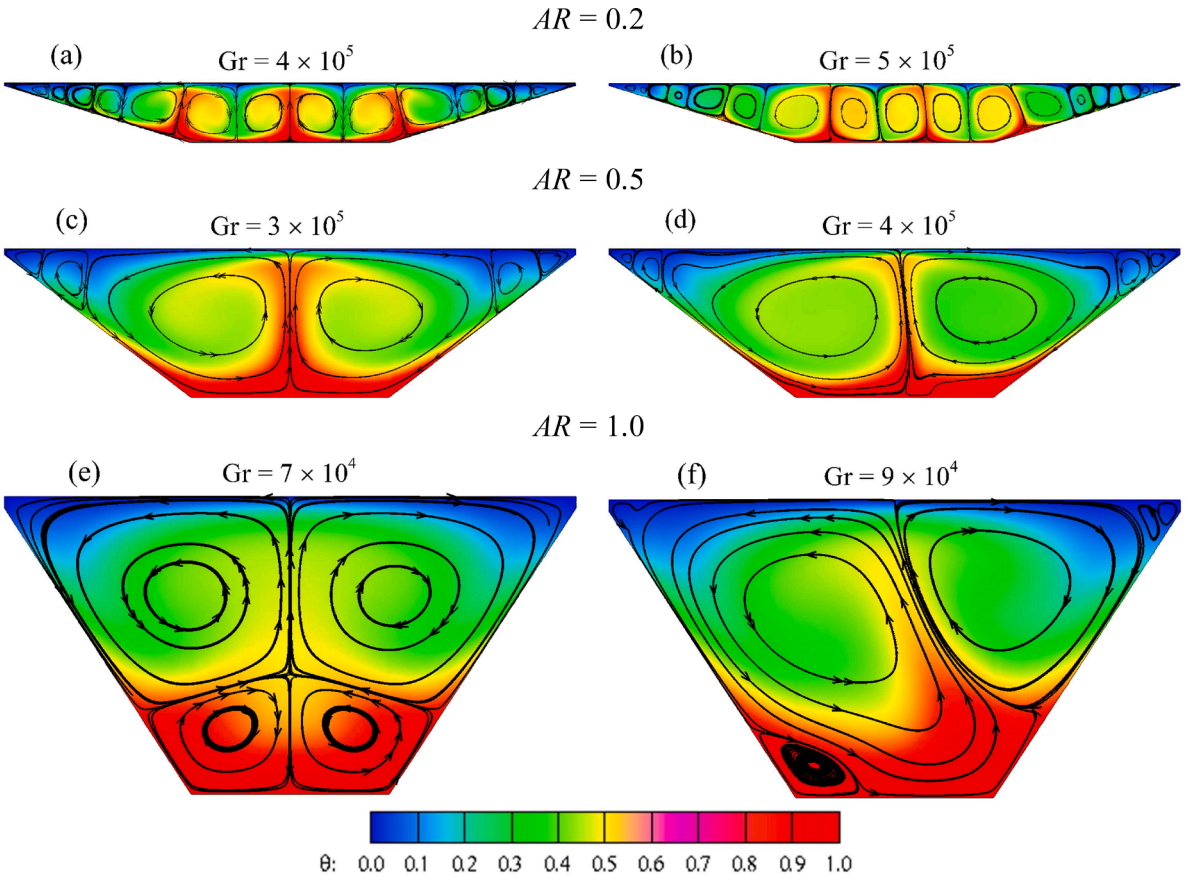

Fig. 5. Streamlines and isotherms to observe the shifting from symmetric to asymmetric state for different aspect ratios.

the study examines how aspect ratios affect HT and S_{gen}. The subsequent sections will proceed to characterize the unsteady NC flow.

4.1. Transition to asymmetrical state

Figs. 4 and 5 show that streamlines and isotherms plotted for different Gr values. As observed in Fig. 4, for lower Gr values (10 to 10^3) across the three *ARs*, NC flow is predominantly governed by conduction. However, convection is enhanced, and additional

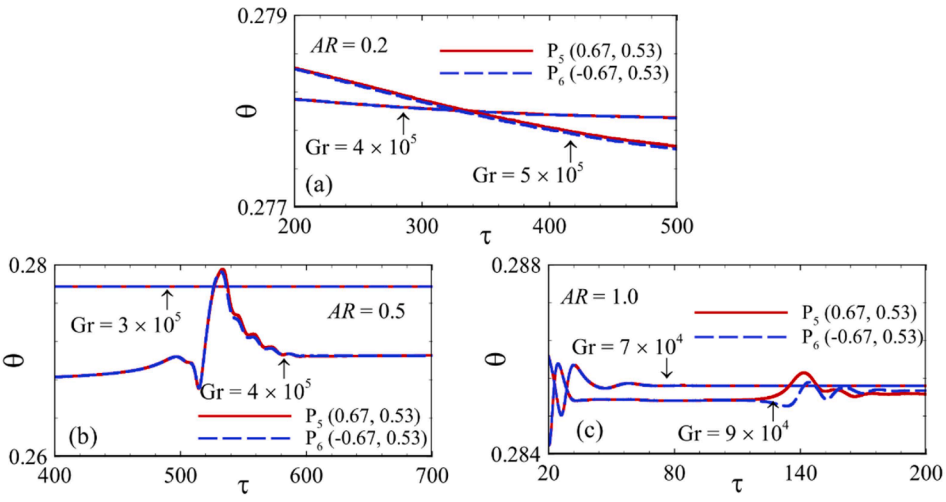

Fig. 6. Temperature time series to observe the Pitchfork bifurcation for different *ARs*.

convective cells are formed only for $AR = 0.2$, at Gr= 10^3. Also, symmetrical steady flow is observed at Gr of 10^4. For the sake of brevity, outcomes for the Gr value 10^4 are omitted here. As Gr values increases, the dominance of buoyancy forces over viscous forces leads to an increase in NC, as shown in Fig. 5. Moreover, both streamlines and isotherms exhibit symmetry along the centerline of the geometry, x= 0, for Gr of 4×10^5 in AR= 0.2; 3×10^5 in AR= 0.5; and 7×10^4 in AR= 1.0. It is widely acknowledged that when Gr exceeds a critical value, typical Rayleigh-Bénard convection occurs. As the Gr value increases, a vigorous and frenetic flow pattern emerges, causing convective cells to break symmetry at x= 0. It is seen that the transition to an asymmetric state occurs at Gr= 5×10^5 in AR= 0.2; Gr= 4×10^5 in AR= 0.5; and Gr= 9×10^4 in AR= 1.0. This marks the initiation of a supercritical pitchfork bifurcation at the critical Gr.

To explain the transition from symmetric to asymmetric state, we analyzed two temperature time series (TTS) at two geometric symmetrical locations, P_5 (0.67, 0.53) and P_6 (-0.67, 0.53) as shown in Fig. 6. In Fig. 6(a), it is evident that the TTS coincide for Gr= 4×10^5 in AR= 0.2 indicating a symmetrical flow with respect to the enclosure's symmetry line. However, for Gr= 5×10^5 in AR= 0.2, the TTS at the two symmetrical locations begins to show differences between τ= 250 and 500. This suggests that a pitchfork bifurcation has occurred, transforming the flow to an asymmetric state. Similarly, in Fig. 6(b), the TTS remain symmetric for Gr = 3×10^5 in AR= 0.5, and a pitchfork bifurcation occurs for Gr= 4×10^5 between τ= 550 and 600. In Fig. 6(c), the TTS remains symmetric for Gr= 7×10^4 in AR= 1.0, and a pitchfork bifurcation occurs for Gr= 9×10^4 between τ= 120 and 200. Therefore, we conclude that the critical Gr increases as the AR decreases during the transition to an asymmetric state.

4.2. Transition to periodic state

To comprehend the changeover from a steady to a periodic state, we examined TTS using spectral analysis. As the Gr rises, the previously asymmetric steady flow evolves into a periodic pattern. At the FDS, the TTS at point P_3 (0, 0.40) reaches a steady state for Gr= 5×10^6, as illustrated in Fig. 7(a). However, when Gr is increased to 6×10^6, the time series of temperature becomes periodic, indicating a Hopf bifurcation between Gr = 5×10^6 and 6×10^6, as portrayed in Fig. 7(b) for an aspect ratio of 0.2. Furthermore, the power spectral density (PSD) of the TTS in Fig. 7(c) demonstrates that the flow oscillates with harmonic modes, with peak frequency f_p = 0.097. A similar spectral analysis was performed for the TTS in the enclosures with aspect ratio of 0.5 and 1.0. Likewise, for an aspect ratio of 0.5, the TTS reaches into a steady state at the FDS for Gr= 6×10^5, and becomes periodic for Gr = 7×10^5, as shown in Fig. 7(d, e). The PSD of the TTS confirms the periodic flow with a peak frequency f_p = 0.169, as portrayed in Fig. 7(f). Similarly, for an aspect ratio of 1.0, the TTS reaches into a steady state at the FDS for Gr = 2×10^6, and becomes periodic for Gr = 3×10^6, as shown in Fig. 7(g, h). The PSD of the TTS confirms the periodic flow with a peak frequency f_p = 0.145, as illustrated in Fig. 7(i). Notably, it's observed that, when AR= 0.5, the convective flow transitions to a periodic state at relatively lower Gr values compared to AR= 0.2 and 1.0.

To enhance the understanding of the Hopf bifurcation mechanism, Fig. 8 illustrates trajectories of limit points and limit cycles in the u-θ plane at point P_2 (0, 0.27) between the time span τ= 900 to 1900. At Gr= 5×10^6, depicted in Fig. 8(a), the (u, θ) trajectory reaches

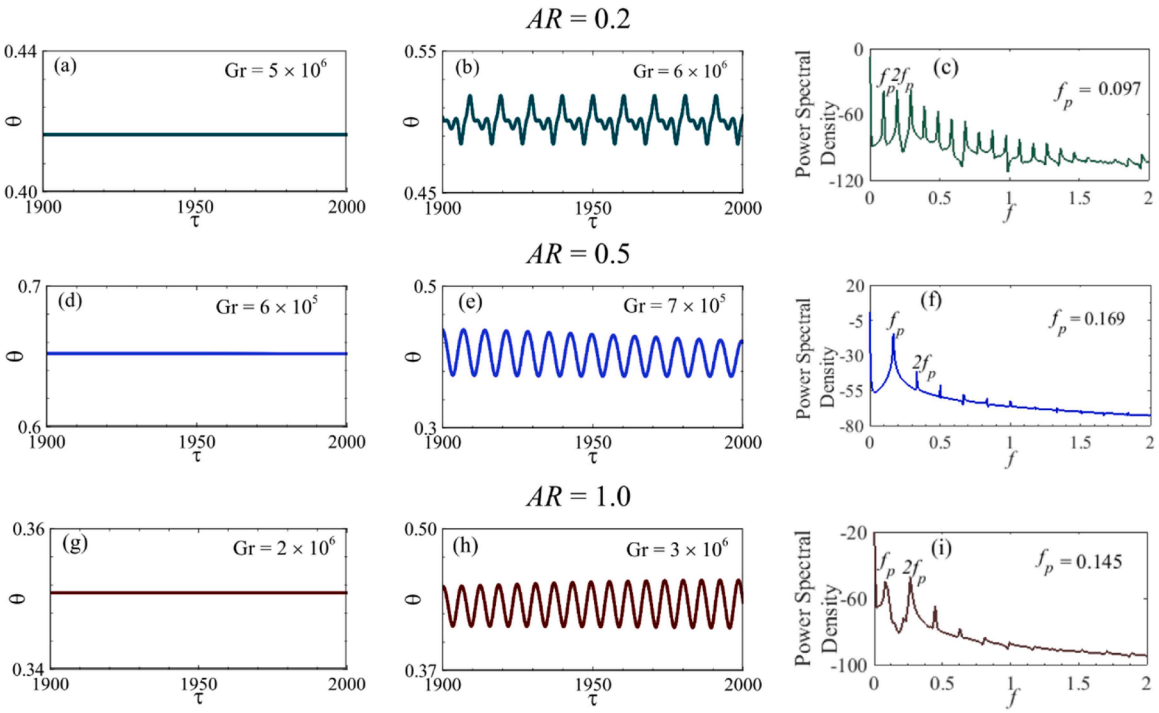

Fig. 7. Temperature time series to observe the shift from steady to periodic state for different aspect ratios at point P_3 (0, 0.40).

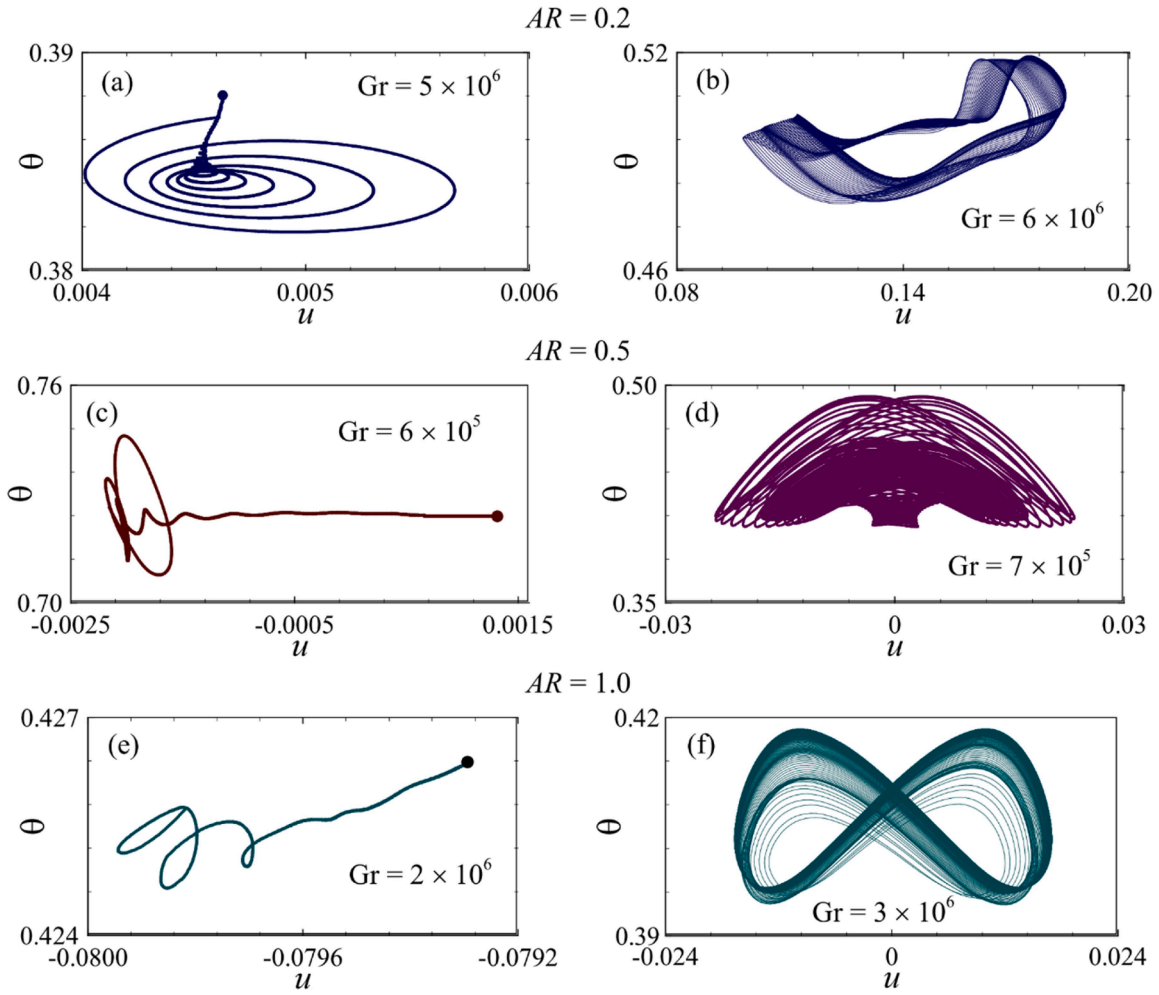

Fig. 8. Limit point and limit cycles at point P_2 (0, 0.27) for different aspect ratio.

a certain static point (indicated by the circular point). In Fig. 8(b), it transitions into a closed limit cycle for Gr= 6×10^6 (depicted by the blackberry orbit). The shift from a limit point to a limit cycle attractor as Gr varies from 5×10^6 to 6×10^6 signifies the occurrence of a Hopf bifurcation within this limit for *AR*= 0.2. For the aspect ratio 0.5, the Hopf bifurcation takes place between Gr of 6×10^5 to 7×10^5. Similarly, for *AR*= 1.0, the Hopf bifurcation occurs between Gr of 2×10^6 to 3×10^6.

4.3. Transition to chaotic state

Consider TTS at point P_3 (0, 0.40) for the higher Gr to distinguish the transition from periodic to a chaotic state. The TTS remains periodic at Gr= 5×10^7, and the PSD of the TTS continues to show a sub-harmonic mode with peak frequency $f_p = 0.0912$, as shown in Fig. 9(a, b). The periodic behavior of the unsteady flow shifts to a chaotic state at Gr = 6×10^7. In this case, the PSD of the TTS reveals that the sub-harmonic mode disappears, and the fundamental peak frequency diminishes, as portrayed in Fig. 9(c, d). In other words, for a cavity with *AR*= 0.2, another bifurcation occurs from a periodic to a chaotic state between Gr values of 5×10^7 and 6×10^7. Similarly, as observed in Fig. 9(e-l), the unsteady flow transitions from a periodic to a chaotic state in the cavity with *AR*= 0.5, between Gr= 4×10^7 and 5×10^7, and in the cavity with *AR*= 1.0, between Gr= 3×10^7 and 4×10^7.

To gain a better understanding of the changeover from periodic to a chaotic state, we examine phase space trajectories in the *u*-θ plane at a fixed point P_4 (0, 0.53), for different *ARs* and Gr values, as depicted in Fig. 10. Notably, distinct limit cycles are observed in Fig. 10(a, c, e), indicating that the unsteady flow remains periodic for Gr= 5×10^7, 4×10^7, and 3×10^7, for the three aspect ratios. This observation aligns with what is shown in Fig. 9(a, e, i). Conversely, the unsteady flow transitions into a chaotic state for Gr= 6×10^7, 5×10^7, and 4×10^7, respectively, for the three aspect ratios, as illustrated in Fig. 10(b, d, f). This finding corresponds with the results presented in Fig. 9(d, h, l). Thus, it is evident that another bifurcation happens, leading the flow from periodic to a chaotic state.

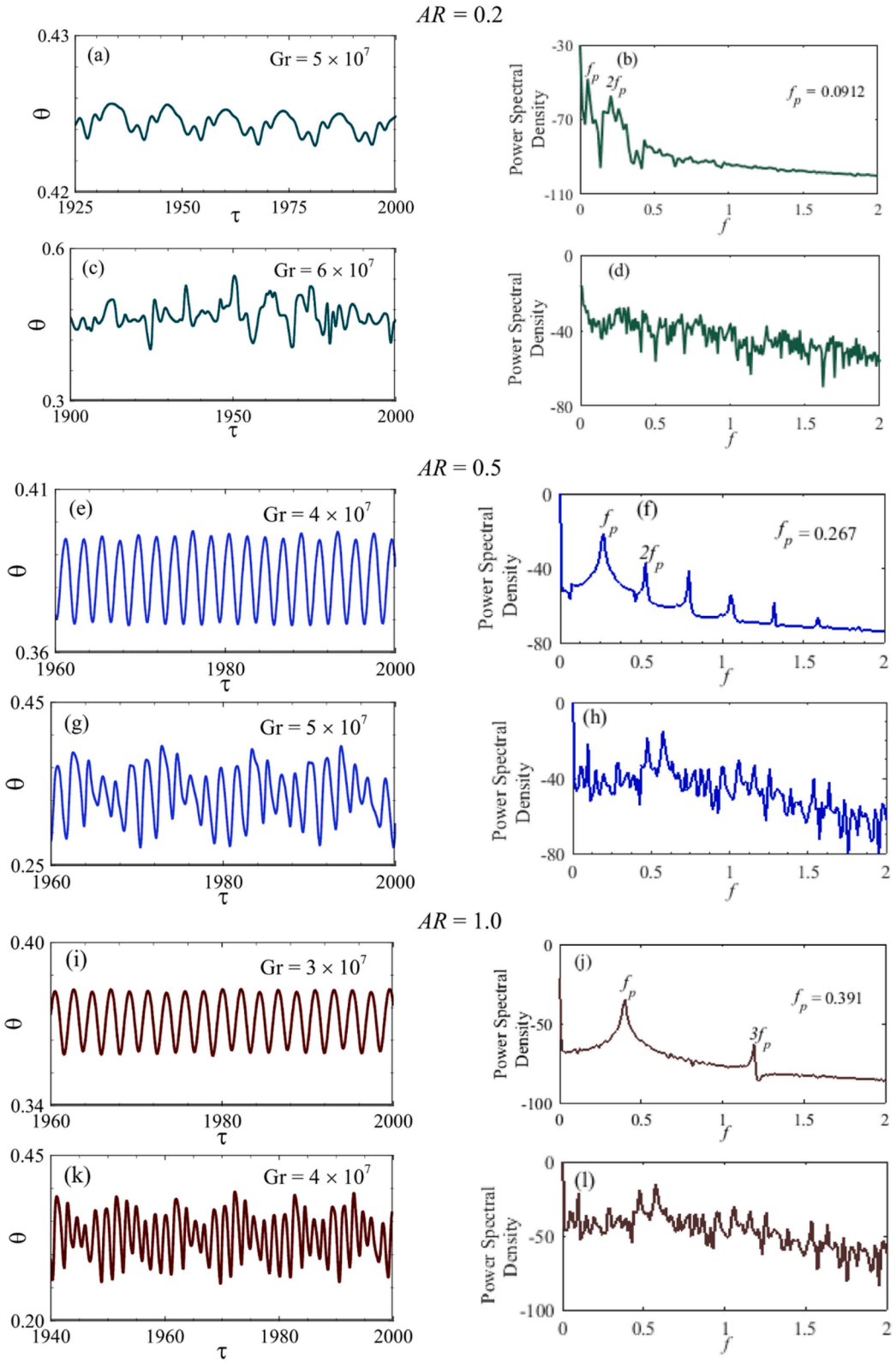

Fig. 9. Temperature time series and PSD to observe the transition from periodic to chaotic state for different aspect ratios at point P_3 (0, 0.40).

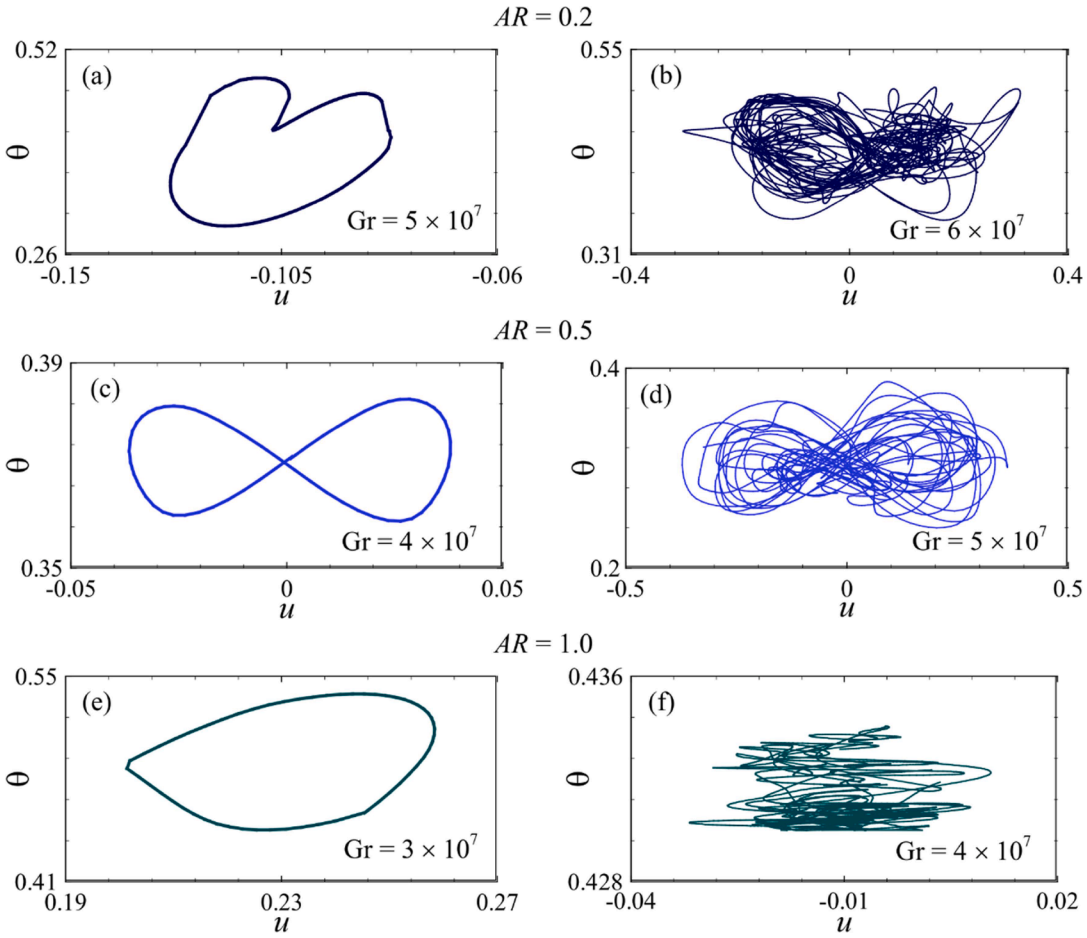

Fig. 10. Phase space trajectory at point P_4 (0, 0.53) for various *ARs*.

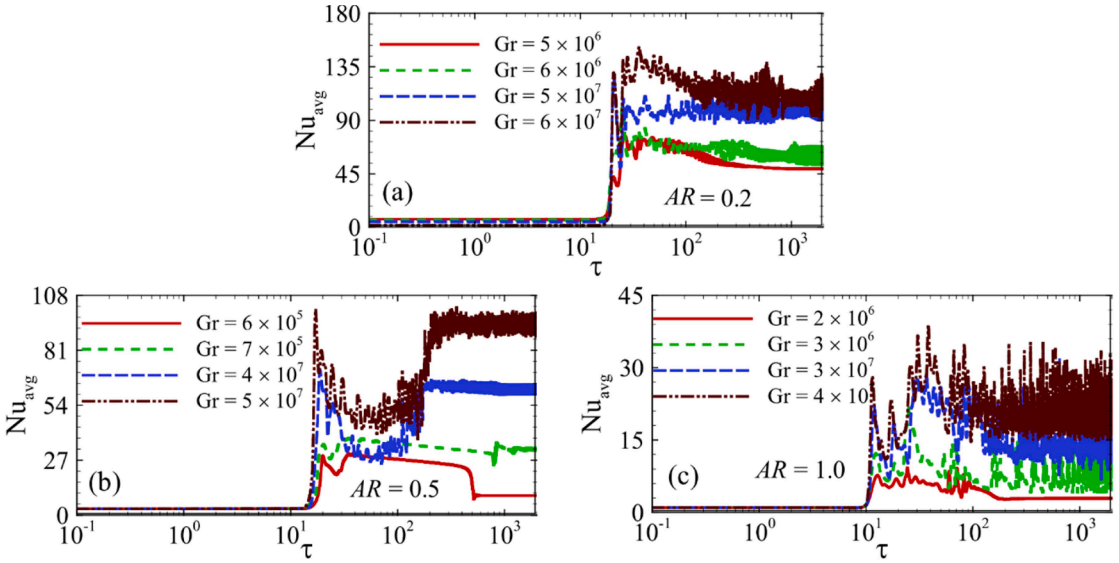

Fig. 11. Average Nusselt number time series to observe HT variation on the different *ARs* at the heated bottom wall.

4.4. Heat transfer

The time series of the averaged Nusselt number (Nu_{avg}), as depicted in Fig. 11, is used to quantify HT through the heated bottom wall, defined in Eq. (7). For the lower Gr values ($Gr \leq 10^5$), HT is dominated by conduction. For brevity, findings for these lower Gr values are omitted. As the cavity is initially occupied by thermally stratified air, the temperature within the cavity differs at the starting point. Therefore, the temperature of the air adjacent to the bottom wall is the equivalent to that of the bottom wall. Initially, the HT from the walls is minimal because of the initially stratified air. At the transitional phase, the stratification diminishes, and the fluctuation of Nu_{avg} values increases as Gr values increases. Moreover, Nu_{avg} time series displays oscillatory behavior all over the transitional stage for higher Gr values due to convection dominance. The Nu_{avg} time series reaches a steady state for $Gr = 5 \times 10^6$ with an enclosure *AR* of 0.2, for $Gr = 6 \times 10^5$ with an enclosure *AR* of 0.5, and $Gr = 2 \times 10^6$ with enclosure *AR* of 1.0. The unsteady flow becomes periodic and maintains its periodic behaviour between $Gr = 6 \times 10^6$ and 5×10^7 with an enclosure *AR* of 0.2; between $Gr = 7 \times 10^5$ and 4×10^7 with an enclosure *AR* of 0.5; and between $Gr = 3 \times 10^6$ and 4×10^7 with an enclosure *AR* of 1.0. Furthermore, the flow becomes chaotic for $Gr = 6 \times 10^7$ with an enclosure *AR* of 0.2; for $Gr = 5 \times 10^7$ with an enclosure *AR* of 0.5; and for $Gr = 4 \times 10^7$ with an enclosure *AR* of 1.0 in the fully evolved stage. In Fig. 11, shows that the quantified Nu_{avg} values increases with the rising of Gr values, demonstrating an augmentation in the HT. It is also observed that the enclosure with $AR = 0.2$ provides the maximum HT compared to other *ARs*.

4.5. Entropy generation

In this section, we investigate entropy generation (S_{gen}) resulting from temperature gradient and fluid friction (FF), as well as local entropy generation (S_t) and local Bejan number (Be_l) as shown in Fig. 12. In the case of lower Gr values (10 to 10^3), the impact of buoyancy force is minimal, and the flow circulation remains consistent. Therefore, conduction effects dominate the fluid flow and the amount of S_{gen}. To be concise, entropy contours are not presented here for Gr= 10 to 10^3. As the Gr value increases, the buoyancy forces driving the convection circulation become stronger, resulting in substantial fluid flow effects; thus, the value of S_t increases. It is observed that with Gr of 10^5, for enclosures with *AR* of 0.2, 0.5, and 1.0, the contours of S_t closely resemble those of S_{gen} due to the temperature gradient. This indicates that for $Gr = 10^5$, S_{gen} due to FF is less significant, and the fluid flow is primarily dominated by S_{gen} due to HT. Conversely, with $Gr = 10^6$, for enclosures with $AR = 0.2$, 0.5, and 1.0, the contours of S_t closely resemble those of S_{gen} due to FF. This indicates that for $Gr = 10^6$, the S_{gen} due to FF is considerably more substantial than S_{gen} due to HT.

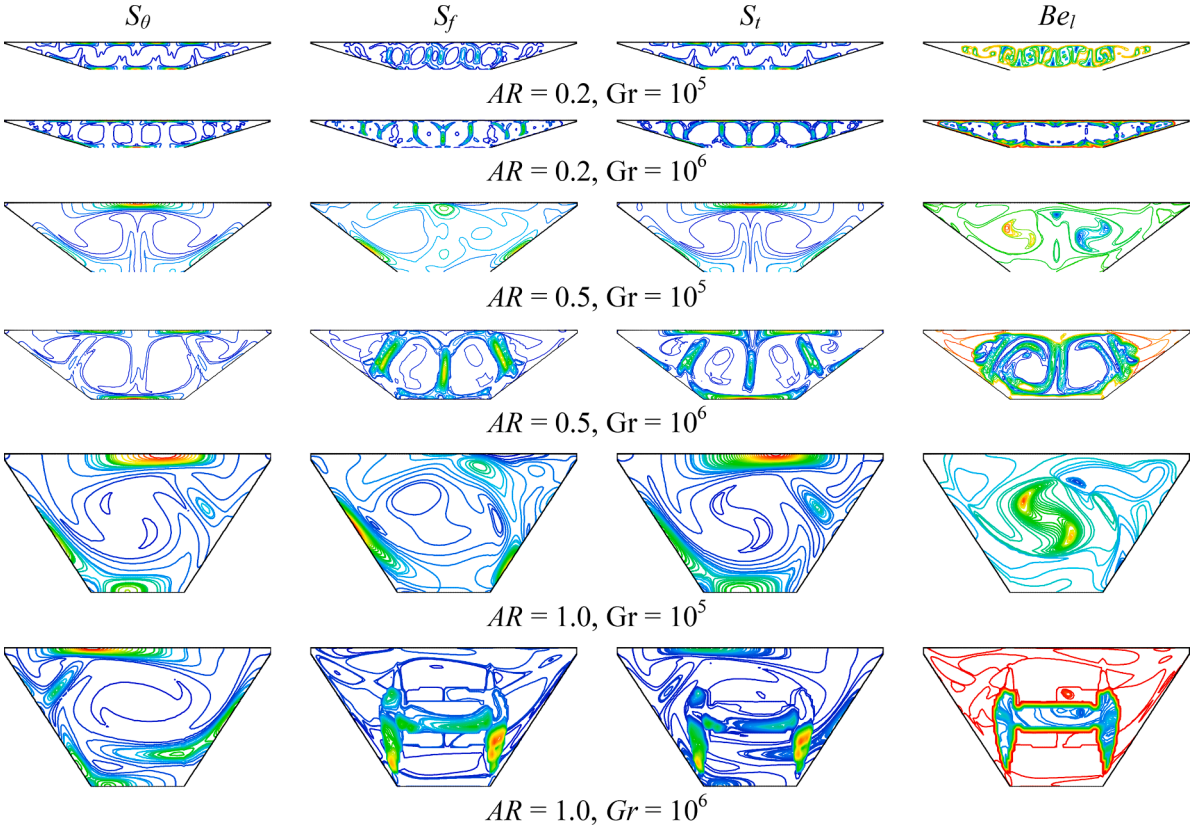

Fig. 12. Distribution of S_{gen} due to HT and FF, local S_{gen}, and Be_l at $Gr = 10^5$ and 10^6 for different *ARs*.

Table 3
The changes of Nu_{avg}, S_{avg} and Be_{avg} with different Gr values for the enclosures with different *ARs*.

Gr	*AR*= 0.2			*AR*= 0.5			*AR*= 1.0		
	Nu_{avg}	S_{avg}	Be_{avg}	Nu_{avg}	S_{avg}	Be_{avg}	Nu_{avg}	S_{avg}	Be_{avg}
10^4	12.95	14.41	0.99	3.39	3.87	0.98	2.66	3.08	0.98
10^5	23.19	30.28	0.88	7.96	15.17	0.85	4.81	10.62	0.83
10^6	39.34	182.64	0.31	27.79	139.29	0.36	8.55	46.34	0.41
10^7	74.59	975.23	0.11	51.57	764.21	0.13	14.13	363.24	0.14
10^8	137.43	3904.26	0.04	105.76	3585.09	0.04	29.53	1498.99	0.05

Table 4
Variation of *ECOP* with different Grashof numbers for the cavity with different *AR*.

Gr	ECOP		
	AR= 0.2	AR= 0.5	AR= 1.0
10^4	0.8986815	0.8759689	0.8636364
10^5	0.7658521	0.5247198	0.4529190
10^6	0.2153964	0.1995118	0.1845058
10^7	0.0764845	0.0674815	0.0388999
10^8	0.0352000	0.0294999	0.0196999

Table 3 illustrates changes in Nu_{avg}, average entropy generation (S_{avg}), and average Bejan number (Be_{avg}) with varying Gr values for enclosures with *AR* of 0.2, 0.5, and 1.0. It is seen that for an enclosure *AR* of 0.2, Nu_{avg} increases from 12.95 to 137.43, and the S_{avg} increases from 14.41 to 3904.26, while Be_{avg} value decreases from 0.99 to 0.04, as Gr rises from 10^4 to 10^8. Conversely, for an enclosure *AR* of 0.5, Nu_{avg} increases from 3.39 to 105.76, S_{avg} increases from 3.87 to 3585.09, and Be_{avg} decreases from 0.98 to 0.04 within the same Gr range. Similarly, for an enclosure *AR* of 1.0, Nu_{avg} increases from 2.66 to 29.53, S_{avg} increases from 3.08 to 1498.99, and Be_{avg} decreases from 0.98 to 0.05 over the same Gr range. This demonstrates that, for all three *ARs*, both Nu_{avg} and S_{avg} value increase while Be_{avg} value decreases with increasing Gr values. For all cases with Gr= 10^4 and 10^5, the Be_{avg} values are greater than 0.5, indicating that S_{gen} due to HT is more significant than S_{gen} due to FF. However, for Gr= 10^6 to 10^8, Be_{avg} is less than 0.5, suggesting that S_{gen} due to FF becomes more dominant than S_{gen} due to HT.

The analysis of *ECOP*, which serves as an indicator of thermal performance within a computational domain, is presented in relation to Gr values for different *ARs* of the enclosure, as displayed in Table 4. A higher value of *ECOP* signifies a reduction in the system's entropy, while a lower *ECOP* value indicates a decrease in HT rate due to thermal convection. During the analysis of these physical quantities, φ and Pr remain constant at 10^{-2} and 0.71, respectively. Furthermore, a wide range of flow monitoring parameters is considered, such as $10^4 \leq Gr \leq 10^8$ and $0.2 \leq AR \leq 1.0$. In our present study, the *ECOP* value decreases as both Gr and *AR* increase. The maximum value of *ECOP*, i.e., 0.89868, is observed when Gr is at its minimum (10^4) with *AR* of 0.2, and the minimum value of *ECOP* is observed when Gr is at its maximum (10^8), with *AR* of 1.0. It suggests that lower Gr values ($\leq 10^5$) result in minimal HT efficiency with lower entropy, which aligns with scenarios where the system operates under relatively stable thermal conditions. Although, HT efficiency may be lower, the system may exhibit more predictable behavior and require less energy input to maintain desired temperatures. On the other hand, higher Gr values ($>10^5$) lead to higher HT rates due to increased thermal buoyancy effects. However, this comes at the expense of increased entropy, introducing challenges such as temperature gradients and potential for thermal instabilities.

5. Conclusions

A comprehensive numerical investigation was conducted to explore the effects of varying *AR* on natural convection and entropy generation within a stratified fluid confined in a trapezoidal enclosure. The enclosure featured thermally stratified side walls, with the top cooled and the bottom heated. Using the Finite Volume Method, the study examined Prandtl number Pr= 0.71 and aspect ratios ranging from 0.2 to 1.0, over a broad spectrum of Grashof numbers from 10 to 10^8.

The simulations highlighted several key bifurcations impacted by aspect ratios and Grashof numbers:

1. The critical Gr for transitioning from symmetric to asymmetric flow was identified as Gr= 5×10^5 for *AR*= 0.2, 4×10^5 for *AR*= 0.5, and Gr= 9×10^4 for *AR* = 1.0.
2. The flow transitioned from steady to periodic behaviour at Gr= 6×10^6 for *AR*= 0.2, Gr= 7×10^5 for *AR*= 0.5, and Gr= 3×10^6 for *AR*= 1.0.
3. The transition from periodic to chaotic behaviour occurred at Gr= 6×10^7 for *AR*= 0.2, Gr= 5×10^7 for *AR*= 0.5, and Gr= 4×10^7 for *AR*= 1.0.

The study also investigated the variations in HT, FF irreversibility and S_{gen} for a trapezoidal cavity with a constant height but varying width. The average Bejan number was utilized to assess the local entropy generation due to HT and FF across the entire cavity.

The findings revealed significant variations in both HT and FF irreversibility concerning *AR*:

- **Low Grashof Numbers (**$Gr \leq 10^5$**)**: HT irreversibility was dominant, with minimal FF irreversibility.
- **High Grashof Numbers (**$Gr > 10^5$**)**: FF irreversibility became dominant, leading to an increase in average entropy generation as the *AR* decreased.

Moreover, the study found that both heat transfer and average entropy generation increased with rising Grashof numbers. Notably, for the same Grashof numbers, the average S_{avg} was lower in cavities with $AR = 1.0$ compared to those with $AR = 0.2$. Increasing the aspect ratio from 0.2 to 1.0 led to a 78.51 % decrease in the average Nusselt number at $Gr = 10^8$. The study concluded that as the aspect ratio increased, the *ECOP* decreased, indicating a reduction in thermodynamics efficiency. This finding underscores the significant influence of *AR* on both local and average entropy generation, highlighting its importance in optimizing thermodynamic efficiency in natural convection and heat transfer processes within engineering systems.

6. Limitations and future works

The present study investigates the effect of aspect ratio on the natural convection heat transfer and entropy generation in trapezoidal cavities with aspect ratio 0.2, 0.5, and 1.0. The Grashof number considered is in the range of 10 to 10^8, with stratified air ($Pr = 0.71$) as the working fluid. This study conducted so far has focused solely on two-dimensional problems. However, the flows with higher Rayleigh numbers, three-dimensional effects could become significant, demanding three-dimensional direct numerical simulations (DNS) on finer grids. Although this is beyond the scope of the current study, it could be an interesting area for future research.

CRediT authorship contribution statement

Md. Mahafujur Rahaman: Writing – original draft, Visualization, Validation, Software, Methodology, Investigation, Formal analysis. **Sidhartha Bhowmick:** Writing – review & editing, Supervision, Conceptualization. **Goutam Saha:** Writing – review & editing. **Feng Xu:** Writing – review & editing. **Suvash C. Saha:** Writing – review & editing, Supervision, Project administration.

Declaration of interests

The authors declare that they have no known competing financial interests or personal relationships that could have appeared to influence the work reported in this paper.

References

[1] D. Angirasa, J. Srinivasan, Natural convection heat transfer from an isothermal vertical surface to a stable thermally stratified fluid, J. Heat. Transf. 114 (1992) 917–923.
[2] D. Angirasa, G.P. Peterson, Natural convection heat transfer from an isothermal vertical surface to a fluid saturated thermally stratified porous medium, Int. J. Heat. Mass Transf. 40 (18) (1997) 4329–4335.
[3] M.A. Hossain, S.C. Paul, A.C. Mandal, Natural convection flow along a vertical circular cone with uniform surface temperature and surface heat flux in a thermally stratified medium, Int. J. Numer. Methods Heat. Fluid. Flow. 12 (3) (2002) 290–305.
[4] W. Lin, S.W. Armfield, P.L. Morgan, Unsteady natural convection boundary-layer flow along a vertical isothermal plate in a linearly stratified fluid with Pr>1, Int. J. Heat. Mass Transf. 45 (2) (2002) 451–459.
[5] A. Shapiro, E. Fedorovich, Unsteady convectively driven flow along a vertical plate immersed in a stably stratified fluid, J. Fluid. Mech. 498 (2004) 333–352.
[6] A. Shapiro, E. Fedorovich, Prandtl number dependence of unsteady natural convection along a vertical plate in a stably stratified fluid, Int. J. Heat. Mass Transf. 47 (22) (2004) 4911–4927.
[7] J. Patterson, J. Imberger, Unsteady natural convection in a rectangular cavity, J. Fluid. Mech. 100 (1) (1980) 65–86.
[8] A.M. Aly, A.J. Chamkha, S.W. Lee, A.F. Al-Mudhaf, On mixed convection in an inclined lid-driven cavity with sinusoidal heated walls using the ISPH method, Comput. Therm. Sci. Int. J. 8 (4) (2016).
[9] S.C. Saha, Unsteady natural convection in a triangular enclosure under isothermal heating, Energy Build. 43 (2-3) (2011) 695–703.
[10] C. Lei, S.W. Armfield, J.C. Patterson, Unsteady natural convection in a water-filled isosceles triangular enclosure heated from below, Int. J. Heat. Mass Transf. 51 (11-12) (2008) 2637–2650.
[11] X. Wen, L.P. Wang, Z. Guo, Development of unsteady natural convection in a square cavity under large temperature difference, Phys. Fluids 33 (8) (2021) 084108.
[12] G.A. Holtzman, R.W. Hill, K.S. Ball, Laminar natural convection in isosceles triangular enclosures heated from below and symmetrically cooled from above, J. Heat Transfer 122 (3) (2000) 485–491.
[13] E.H. Ridouane, A. Campo, Formation of a pitchfork bifurcation in thermal convection flow inside an isosceles triangular cavity, Phys. Fluids 18 (7) (2006) 074102.
[14] E.F. Kent, Laminar natural convection in isosceles triangular roofs in wintertime conditions, Heat Transf. Eng. 31 (13) (2010) 1068–1081.
[15] S.C. Saha, J.C. Patterson, C. Lei, Natural convection and heat transfer in attics subject to periodic thermal forcing, Int. J. Therm. Sci. 49 (10) (2010) 1899–1910.
[16] S.C. Saha, Y. Gu, Transient air flow and heat transfer in a triangular enclosure with a conducting partition, Appl. Math. Modell. 38 (15-16) (2014) 3879–3887.
[17] S.C. Saha, Y. Gu, Natural convection in a triangular enclosure heated from below and non-uniformly cooled from top, Int. J. Heat. Mass Transf. 80 (2015) 529–538.
[18] A. Sojoudi, S.C. Saha, F. Xu, Y. Gu, Transient air flow and heat transfer due to differential heating on inclined walls and heat source placed on the bottom wall in a partitioned attic shaped space, Energy Build. 113 (2016) 39–50.
[19] X. Wang, S. Bhowmick, Z.F. Tian, S.C. Saha, F. Xu, Experimental study of natural convection in a V-shape-section cavity, Phys. Fluids 33 (1) (2021) 014104.
[20] H. Cui, F. Xu, S.C. Saha, Q. Liu, Transient free convection heat transfer in a section-triangular prismatic enclosure with different aspect ratios, Int. J. Therm. Sci. 139 (2019) 282–291.
[21] S.C. Saha, A.M. Sefidan, A. Sojoudi, Unsteady natural convection within an attic-shaped space subject to sinusoidal heat flux on inclined walls, Energy Eng. J. Assoc. Energy Eng. 117 (2020) 1–17.

[22] A.M. Aly, S.W. Lee, N. Alsedais, The magnetic field on the bioconvection flow of NEPCM in a z-shaped cavity containing three circular cylinders, Chin. J. Phys. (2024), https://doi.org/10.1016/j.cjph.2024.07.012.
[23] W. Alhejaili, A.M. Aly, Artificial intelligence and numerical simulations for Cattaneo–Christov heat and mass fluxes of nano-encapsulated phase change materials in a zigzag porous cavity, J. Energy Storage 90 (2024) 111750.
[24] W. Alhejaili, P. Pandey, A.M. Aly, Incompressible smoothed particle hydrodynamics simulations enhanced by hybrid artificial intelligence for investigating magnetic field influence on double diffusion in an arc-shaped cavity, Numer. Heat Transf. Part A Appl. (2024) 1–24.
[25] M.T. Nguyen, A.M. Aly, S.W. Lee, A numerical study on unsteady natural/mixed convection in a cavity with fixed and moving rigid bodies using the ISPH method, Int. J. Numer. Methods Heat. Fluid. Flow. 28 (3) (2018) 684–703.
[26] L. Iyican, Y. Bayazitoglu, L.C. Witte, An analytical study of natural convective heat transfer within a trapezoidal enclosure, J. Heat Transf. 102 (1980) 640–647.
[27] L. Iyican, L.C. Witte, Y. Bayazitoglu, An experimental study of natural convection in trapezoidal enclosures, J. Heat. Transf. 102 (3) (1980) 648–653.
[28] E. Natarajan, S. Roy, T. Basak, Effect of various thermal boundary conditions on natural convection in a trapezoidal cavity with linearly heated side wall (s), Numer. Heat Transf. Part B Fundam. 52 (6) (2007) 551–568.
[29] E. Natarajan, T. Basak, S. Roy, Natural convection flows in a trapezoidal enclosure with uniform and non-uniform heating of bottom wall, Int. J. Heat. Mass Transf. 51 (3-4) (2008) 747–756.
[30] K. Lasfer, M. Bouzaiane, T. Lili, Numerical study of laminar natural convection in a side-heated trapezoidal cavity at various inclined heated sidewalls, Heat Transfer Eng. 31 (5) (2010) 362–373.
[31] Y. Varol, Natural convection for hot materials confined within two entrapped porous trapezoidal cavities, Int. Commun. Heat Mass Transf. 39 (2) (2012) 282–290.
[32] E. Fontana, A.D. Silva, V.C. Mariani, F. Marcondes, The influence of baffles on the natural convection in trapezoidal cavities, Numer. Heat Transf. Part A Appl. 58 (2) (2010) 125–145.
[33] M.M. Gholizadeh, R. Nikbakhti, J. Khodakhah, A. Ghasemi, Numerical study of double diffusive buoyancy forces induced natural convection in a trapezoidal enclosure partially heated from the right sidewall, Alex. Eng. J. 55 (2) (2016) 779–795.
[34] K.G.B.M. Gowda, M.S. Rajagopal, K.N. Seethramu, Numerical studies on natural convection in a trapezoidal enclosure with discrete heating, Heat Transf. Eng. 41 (2019) 595–606.
[35] M.M. Rahaman, R. Titab, S. Bhowmick, R.N. Mondal, S.C. Saha, Unsteady 2D flow in an initially stratified air-filled trapezoid, Jagannath Univer. J. Sci. 8 (2022) 1–6.
[36] M.M. Rahaman, S. Bhowmick, R.N. Mondal, S.C. Saha, Unsteady natural convection in an initially stratified air-filled trapezoidal enclosure heated from below, Processes 10 (7) (2022) 1383.
[37] M.M. Rahaman, S. Bhowmick, R.N. Mondal, S.C. Saha, A computational study of chaotic flow and heat transfer within a trapezoidal cavity, Energies (Basel) 16 (13) (2023) 5031.
[38] M.M. Rahaman, S. Bhowmick, B.P. Ghosh, F. Xu, R.N. Mondal, S.C. Saha, Transient natural convection flows and heat transfer in a thermally stratified air-filled trapezoidal cavity, Therm. Sci. Eng. Progr. 47 (2024) 102377.
[39] A. Bejan, Entropy Generation through Heat and Fluid Flow, Wiley & Sons, New York, 1994.
[40] A. Bejan, Entropy Generation Minimization, CRS Press, Boca Raton, 1996.
[41] L. Berrin Erbay, Z. Altaç, B. Sülüş, Entropy generation in a square enclosure with partial heating from a vertical lateral wall, Heat Mass Transf. 40 (12) (2004) 909–918.
[42] M. Alipanah, P. Hasannasab, S.F. Hosseinizadeh, M. Darbandi, Entropy generation for compressible natural convection with high gradient temperature in a square cavity, Int. Commun. Heat Mass Transf. 37 (9) (2010) 1388–1395.
[43] G.G. Ilis, M. Mobedi, B. Sunden, Effect of aspect ratio on entropy generation in a rectangular cavity with differentially heated vertical walls, Int. Commun. Heat Mass Transf. 35 (6) (2008) 696–703.
[44] L. Kuddusi, First and second law analysis of fully developed gaseous slip flow in trapezoidal silicon microchannels considering viscous dissipation effect, Int. J. Heat. Mass Transf. 54 (1-3) (2011) 52–64.
[45] T. Basak, A.K. Singh, T.A. Sruthi, S. Roy, Finite element simulations on heat flow visualization and entropy generation during natural convection in inclined square cavities, Int. Commun. Heat Mass Transf. 51 (2014) 1–8.
[46] M.M. Rahaman, S. Bhowmick, R.N. Mondal, S.C. Saha, Transient 2D flow in a stratified air-filled trapezoidal cavity, Available at SSRN 4874263 (2024).
[47] J.H. Saboj, P. Nag, G. Saha, S.C. Saha, Entropy production analysis in an octagonal cavity with an inner cold cylinder: a thermodynamic aspect, Energies (Basel) 16 (14) (2023) 5487.
[48] K.B. Saleem, A.K. Alshara, Natural convection in a triangular cavity filled with air under the effect of external air stream cooling, Heat Transf. Asian Res. 48 (7) (2019) 3186–3213.
[49] S. Bhowmick, F. Xu, X. Zhang, S.C. Saha, Natural convection and heat transfer in a valley shaped cavity filled with initially stratified water, Int. J. Therm. Sci. 128 (2018) 59–69.
[50] S. Bhowmick, S.C. Saha, M. Qiao, F. Xu, Transition to a chaotic flow in a V-shaped triangular cavity heated from below, Int. J. Heat. Mass Transf. 128 (2019) 76–86.
[51] S. Bhowmick, F. Xu, M.M. Molla, S.C. Saha, Chaotic phenomena of natural convection for water in a V-shaped enclosure, Int. J. Therm. Sci. 176 (2022) 107526.